Droplet size distributions as a function of rainy system type and cloud condensation nuclei concentrations

Micael A. Cecchini[1], Luiz A. T. Machado[1], Paulo Artaxo[2]

[1] Instituto Nacional de Pesquisas Espaciais (INPE), Centro de Previsão de Tempo e Estudos Climáticos (CPTEC) – Brazil

[2] Instituto de Física (IF), Universidade de São Paulo (USP)

Accepted for publication at Atmos. Res.

February, 2014

ABSTRACT

This work aims to study typical droplet size distributions (DSDs) for different types of precipitation systems and cloud condensation nuclei concentrations over the Vale do Paraíba region in southeastern Brazil. Numerous instruments were deployed during the CHUVA (Cloud processes of tHe main precipitation systems in Brazil: a contribUtion to cloud resolVing modeling and to the GPM) Project in Vale do Paraíba campaign, from November 22, 2011, through January 10, 2012. Measurements of CCN (Cloud Condensation Nuclei) and total particle concentrations, along with measurements of rain DSDs and standard atmospheric properties, including temperature, pressure and wind intensity and direction, were specifically made in this study. The measured DSDs were parameterized with a gamma function using the moment method. The three gamma parameters were disposed in a 3-dimensional space, and subclasses were classified using cluster analysis. Seven DSD categories were chosen to represent the different types of DSDs. The DSD classes were useful in characterizing precipitation events both individually and as a group of systems with similar properties. The rainfall regime classification system was employed to categorize rainy events as local convective rainfall, organized convection rainfall and stratiform rainfall. Furthermore, the frequencies of the seven DSD classes were associated to each type of rainy event. The rainfall categories were also employed to evaluate the impact of the CCN concentration on the DSDs. In the stratiform rain events, the polluted cases had a statistically significant increase in the total rain droplet concentrations (TDC) compared to cleaner events. An average concentration increase from 668 cm^{-3} to 2012 cm^{-3} for CCN at 1% supersaturation was found to be associated with an increase of approximately 87 m^{-3} in TDC for those events. For the local convection cases, polluted events presented a 10% higher mass weighted mean diameter (D_m) on average. For the organized convection events, no significant results were found.

1. Introduction

Clouds are recognized as one of the most important components of Earth's system because they persistently cover over half of its surface area and have large impacts on the radiative balance and water cycle (IPCC, 2007). Cloud droplets can only be formed in specific atmospheric thermodynamic conditions through the condensation of water vapor onto an aerosol particle, which, given certain conditions, dilutes into the liquid water, and the solute grows to form a cloud droplet (Köhler, 1936; Petters and Kreidenweis, 2007; Petters and Kreidenweis, 2013). Numerous studies have focused on aerosol-cloud interactions through both observational (Rosenfeld, 2000; Heymsfield and McFarquhar, 2001; Andrae et al., 2004; Rosenfeld et al., 2008) and modeling (van den Heever et al., 2006, 2011; Lee et al., 2008; Storer et al., 2010; Morrison, 2012; Igel et al., 2013; Storer and van den Heever, 2013) experiments. It is generally agreed that aerosols have significant effects on cloud microphysical properties, including droplet mean diameters and number concentrations (McFiggans et al., 2006, Freud et al., 2008), which in turn can affect its radiative properties and the Earth's climate (Twomey, 1974; Albrecht, 1989; Lohmann and Feichter, 2005). However, there are still controversial results regarding aerosol-cloud-precipitation interactions, e.g., the effect of enhanced particle loading on rainfall, cloud liquid water path (LWP) and cloud fraction (CF). Quaas et al. (2008) and Quaas et al. (2009), using satellite and global climate model (GCM) data, reported an increase in both LWP and CF following an increase in aerosol loading. The extent to which these effects on cloud properties are actually due to the increase in particle concentrations as opposed to other factors, e.g., changes in the humidity profile, satellite retrieval uncertainty and/or local meteorology, remains a topic of debate. Loeb and Shuster (2008) argued that local meteorology can play an important role in both aerosol concentration and cloud cover, which could explain the positive relationship between aerosol optical depth (AOD) and cloud cover observed in some studies. They limited the analysis to a small region (5° latitude x 5° longitude) and selected only satellite retrievals with similar meteorological conditions. However, they still found a positive relationship between AOD and CF. To avoid satellite retrieval issues, Grandey et al. (2013) utilized AOD data from a global model with detailed aerosol microphysics, i.e., the Monitoring Atmospheric Composition and Climate (MACC) reanalysis-forecast. They showed that a large portion of the positive relationship between AOD and CF found in satellite studies could most likely be explained by cloud contamination and retrieval issues. By utilizing AOD data from the reanalysis-forecast system, the authors found weaker aerosol effects on cloud cover.

More notably, they reported negative AOD-CF correlations in the tropics, largely due to the wet scavenging effect, which is not captured by satellite data. Regarding the cloud liquid water content, Ackerman et al. (2004) found a negative correlation with increased aerosol loading. These previous authors ran simulations with detailed cloud microphysics and found that the variation of liquid water content with increasing particle concentrations is a result of the balance between a moistening effect of decreased rainfall and a drying effect generated from intensified entrainment. Therefore, they suggested that there is not a direct correlation between aerosol loading and cloud liquid water content, which should apply for other cloud properties, e.g., CF or even rainfall. Other studies that found negative relations between aerosol loading and cloud liquid water content include Twohy et al. (2005) and Lee et al. (2009).

Regarding aerosol influences on rainfall, contrasting results have also been reported in the literature. Khain (2009) provided a general review of the issue, highlighting important mechanisms in aerosol-cloud-precipitation interactions. The author claims that opposing aerosol effects on precipitation presented in the literature occur due to the different precipitating systems and meteorological regimes being analyzed. Through a review of many previous studies, it was found that an increase in aerosol loading could have both positive and negative effects on total rainfall; the sign and intensity of such an impact is defined by meteorological conditions and cloud/system type. For example, the author suggests that humidity plays a major role in determining aerosol effects on precipitation, where moist environments favor an increase in rainfall for polluted clouds and dry air tends to favor the suppression of rain in high particle loading conditions. The author ran simulations with a 2D model including bin microphysics to confirm these conclusions. The development of bin microphysics models, together with bulk microphysics schemes, is an indication that a more detailed description of cloud development is needed to close gaps in our understanding of aerosol-cloud-precipitation interactions.

Studying aerosols-cloud-precipitation interactions through direct in-situ measurements of particle concentrations and surface precipitation characteristics is an approach that is not often observed in the literature. This approach permits detailed observations of individual precipitation events. However, statistical and geographical representations of the phenomena involved are lost. Nevertheless, detailed knowledge of the precipitation DSD evolution and its dependence on the precipitation regime is very important for testing and parameterizing cloud resolving and bin microphysics models, as well as remote sensing estimates of cloud/precipitation properties. For example, a common strategy to relate radar reflectivity to rainfall rate is the application of a determined Z-R relationship (where Z is the reflectivity and R the rain rate) as initially proposed by

Marshall and Palmer (1948). However, the use of such a fixed relationship is subject to various sources of error, one of them being the great DSD spatial and temporal variability (e.g. Smith 1993; Smith and De Veaux 1994) which may require various Z-R relationships. Observations show that different precipitating systems require different Z-R relations (Steiner and Smith, 2000) and even within the same system there could be variability (Uijlenhoet et al., 2003). As aerosols are capable of altering cloud and precipitation DSD, as suggested by the previously cited works, they could also influence the Z-R relations, highlighting the importance of aerosol-cloud-precipitation DSD studies.

For the modeling of clouds, direct measurements of cloud/precipitation DSDs are useful for validating and improving bulk microphysical models. One way to parameterize DSDs is through the moment method described in Tokay and Short (1996). This method describes a DSD with three parameters representing its shape, width and intercept. In this way, the problem is reduced to 3 variables describing the DSD. The 3-dimension space containing the 3 gamma parameters can be used to study the DSD types and their variability. This study proposes to introduce a new methodology to study the DSD characterization by applying cluster analysis to the gamma function parameters. Based on this description, this study proposes an association of the DSD classes to precipitation regimes and aerosol loadings. The goal for this study is to understand the impact of rain types and CCN concentrations on the DSD statistical population.

Section 2 describes the procedures for the collection of experimental data and measurement strategy. Sections 3 and 4 show the methods applied to achieve the results outlined in section 5. Finally, section 6 summarizes our major findings.

2. Experiment design and data

Extensive aerosol and precipitation measurements were taken during the CHUVA GLM - *Vale do Paraíba* experiment that spanned from November 2011 to March 2012. This was the fourth experiment of the “Cloud processes of tHe main precipitation systems in Brazil: a contribUtion to cloud resolVing modeling and to the GPM (GlobAl Precipitation Measurement)” (CHUVA) campaign. The CHUVA project aims to better characterize Brazilian precipitating systems through intensive observational and modeling studies over strategic locations representing the main precipitation regimes (see Machado et al., 2013 for a detailed description). On the Vale do Paraíba experiment the main focus was the observation of lightning activity over the region, with several electric field and

lightning sensors including a Lightning Mapping Array (LMA) system. For the detection of cloud/precipitation characteristics, the experiment makes use of radiometers (MP3000A from Radiometrics), acoustic disdrometers (Joss-Waldvogel RD-80 from Disdromet Ltd.), laser disdrometers (Parsivel from Ott. Inc.) rain gauges, a vertical poiting radar (MRR-2 from METEK) and a X-Band radar (Meteor 50DX from Gematronik). Seven stations were deployed from São José dos Campos until the coast, forming a perpendicular line with it. In all those stations there was at least one disdrometer, one rain gauge and one GPS available.

To supplement the data collected by CHUVA at Vale do Paraíba, two aerosol/CCN counters where deployed. A *TSI Inc.* Condensation Particle Counter model 3772 (CPC) measured total particle number concentrations greater than 7 nm in diameter, while a *Droplet Measurements Technology* Cloud Condensation Nuclei Counter (CCNC Roberts and Nenes, 2005) counted activated droplets at 0.2, 0.4, 0.6, 0.8 and 1.0% supersaturations. The CPC and CCNC instruments were deployed inside a container at the Institute for Advanced Studies (IEAv) in the country side of São José dos Campos, a medium-sized city located approximately 100 Km northeast of São Paulo. An inlet positioned 3 meters above the ground was connected to the CPC and CCNC through a copper tube. Both instruments operated fairly continuously with occasional breakdowns due to regional power supply issues. The CPC instrument provides total particle counts every 5 minutes, and the CCNC takes 20 minutes to measure CCN concentrations at all five supersaturations.

Although there was a wide array of instruments available, this work focuses on observations of $CCN_{1.0}$ concentrations (particles activated at 1.0% supersaturation) and rain droplet size distributions (DSDs) from the Joss-Waldvogel disdrometer (JWD). Therefore, a more detailed (precipitation) event-centric analysis was possible. The JWD instrument has a refresh rate of 1 measurement every minute that consists of a DSD divided into 20 *bins* between 0.359 mm and 5.373 mm. *Bin* sizes grow exponentially with the droplet diameter. The accuracy of droplet concentrations is about 5%. Tokay et al. (2001) have made a comparison between video disdrometers and the JWD, showing that those instruments measure consistently the DSD. The main differences are on the lower-end side of the DSD (i.e. for the small droplets), in which case the video disdrometer counted significantly more droplets. Both kinds of instruments tend to underestimate total accumulated rain, with the JWD providing the lowest values. However, rain rates and reflectivity calculated from those instruments are fairly similar (Tokay et al., 2001). Leinonen et al. (2012) performed a validation of JWD data in a five years period, comparing the measured DSD with other

hydrometeor-sizing instruments, highlighting the robustness of the information provided by the impact disdrometer. During the CHUVA-Vale do Paraíba measurement period, the JWD collected a total of 7004 DSDs, which accounted for a total rainfall of 296 mm.

3. Methodology

The DSD measurements were parameterized following Tokay and Short, 1996, by obtaining the DSD third, fourth and sixth moments using

$$M_x = \int_0^\infty D^x N(D) dD, \quad (1)$$

where M_x is the *x*-th moment of the DSD, represented by N(D), and D is the droplet diameter. The measured DSDs were fitted gamma distributions in the form

$$N(D) = N_0 D^m \exp(-\Lambda D), \quad (2)$$

where N_0 is the DSD intercept, *m* is the shape parameter and Λ is the curvature. The three gamma fit parameters (N_0, *m* and Λ) were obtained as follows:

$$m = \frac{11G-8+[G(G+8)]^{1/2}}{2(1-G)}, G = \frac{M_4^3}{M_3^2 M_6}, \quad (3)$$

$$N_0 = \frac{\Lambda^{m+4} M_3}{\Gamma(m+4)}, \quad (4)$$

$$\Lambda = \frac{(m+4)M_3}{M_4} = \frac{(m+4)}{D_m}, \quad (5)$$

where Γ is the gamma function and D_m is the mass-weighted mean rain droplet diameter given by the ratio of the fourth and third moments. The parameter *m* is non-dimensional, while N_0 and Λ have units of $mm^{-1-m}m^{-3}$ and mm^{-1}, respectively. Note that the *m* in the units of N_0 is the value of the parameter *m*, not meters.

Other important parameters analyzed were the zeroth moment (i.e., TDC – Total Droplet Concentration, also obtained from Equation 1) and rain intensity (RI). RI is defined as follows:

$$RI = 6\pi \times 10^{-6} \int_0^\infty V(D) D^3 N(D) dD. \quad (6)$$

where V(D) is the terminal velocity of rain droplets (cm/s) with diameter D (mm). The terminal velocities were tabulated by the manufacturer for the 20 *bins* of the

disdrometer, based on the study of Gunn and Kinzer (1949). TDC is given in m^{-3} and RI is in mm/h.

By parameterizing all the DSD measurements, some instability was observed in the gamma-fitted results, associated primarily with small RI data. Therefore, a filter was applied that essentially eliminated all parameterized DSDs with RI < 1 mm/h, $N_0 < 10^{-10}$ and $N_0 > 10^{20}$. Approximately 74% of the measured DSDs were discarded, although 262 mm of total rainfall was retained, corresponding to 88% of the total accumulated rain. All these cases were associated with very light rainfall, where the applied methodology is not well adapted.

A 3-dimensional sub-space was defined for N_0, *m* and Λ in the *x*, *y* and *z* directions, respectively, permitting the initialization of the cluster analysis. To do so, adjustments were applied to each gamma parameter to achieve a similar range interval. This procedure allowed the three axes to have nearly the same contribution in the cluster procedure. N_0, with the highest numerical values, was adjusted to twice its logarithmic scale. To have the same dynamic variation, the *m* values were divided by two so that most of the parameter values were approximately between 0 and 30. The k-means clustering method was utilized as described by Kanungo et al. (2002). The general concept of k-means clustering is to identify a certain number of groups of data (or clusters) in the k-dimensional space defined by k parameters, minimizing the Euclidean distance between them. For the case of the gamma fit parameters, k was defined to be 3. The number of clusters identified can be automatically calculated or defined prior to the algorithm run. Several tests were conducted and it was noted that predefining 7 clusters was ideal for representing the set of analyzed data.

3.1 The precipitation type classification

To identify precipitating systems that were formed in similar thermodynamic environments, daily patterns of atmospheric conditions were defined for each rainy day. These patterns were defined based on the general characteristics of each day in the measurement period (Figure 1). ΔT and $\Delta CCN_{1.0}$ correspond to the daily amplitudes of temperature and $CCN_{1.0}$ concentrations, respectively, while RI_m is the mean rain intensity for the day, as measured by the disdrometer (before applying any filtering). The amplitude of $CCN_{1.0}$ concentrations (maximum minus minimum concentrations for the day) was found to be associated with precipitating system type. Higher values of

this amplitude were frequently associated with convective systems, as the atmospheric instability favors both vertical transport of particles and the formation of convective clouds. On the other hand, stratiform systems hamper increases in $CCN_{1.0}$ concentrations by both cleaning the atmosphere with persistent rain and by suppressing vertical transport. Although the classification method is efficient for isolating similar environments and precipitating systems, it is quite simple. Days with persistent rain favor low ΔT and low $\Delta CCN_{1.0}$ because clouds block the incoming solar radiation and the air is cleaned by rainout/washout effects. Therefore, by applying the thresholds of $\Delta T \leq 7$°C and $\Delta CCN_{1.0} \leq 3500$ cm^{-3}, it is possible to isolate days with persistent rain. The days that were characterized by light rain ($RI_m < 1$ mm/h) were classified as Stratiform Rain, while $RI_m \geq 1$ mm/h was chosen to classify Organized Convection days. Days that were favorable to produce convective rain had larger ΔT and $\Delta CCN_{1.0}$ because a clearer sky in the morning and early afternoon is typically present, followed by relatively strong rainfall in the late afternoon/early night. For this configuration, Local Convection days were identified when the longest event on each day did not last longer than 2 hours. Moreover, a rainfall event with longer duration indicates an Organized Convection day. It is important to note that the limits imposed on ΔT, $\Delta CCN_{1.0}$, RI_m and rain duration are only valid for the region of interest during the experiment period and studied configuration; it is not advised to apply this classification system to other locations/seasons. The idea is to identify similar events and analyze their differences based on relative variations in $CCN_{1.0}$ concentration. For instance, the Local Convection events can be ordered based on their respective associated $CCN_{1.0}$ concentrations, so the relatively polluted and pristine ones can be identified. The methodology used to compare relatively polluted and pristine events is further detailed in section 4.

4. The aerosol and precipitation interaction

Precipitation events were defined by the timing of measured DSDs. When the interval between two DSDs was at least 20 minutes, a new event was defined. $CCN_{1.0}$ associated with each event was calculated as 2-hour averages (from 2.5 hours to 30 minutes prior to the rain initiation). Only the first event in each day was selected to eliminate rainout and washout effects on the analysis. Moreover, all events that lasted less than 10 minutes and didn't have associated $CCN_{1.0}$ (due to sampling issues) were eliminated from the analysis. Considering these requirements, 6 Local Convection, 5

Stratiform Rain and 5 Organized Convection rain events were classified. For each classification, the averaged RI, TDC and D_m were computed for the 2 most polluted and 2 most pristine cases. In order to confirm that the polluted and pristine DSDs were actually different, those DSD parameters were compared and the results were subjected to Student t-tests to assess the statistical significance. Ideally, this comparison requires 2 samples consisting of independent data. However, it was noted that the one-minute DSD parameters were auto correlated, so the tests had to be carried out taking that into account. Guidelines suggested by Zwiers and Storch (1995) were followed.

The differences between the polluted and pristine DSD parameters were tested based on

$$t = \frac{\overline{x_1} - \overline{x_2}}{s\left[1/\left(n_{1_e}\right)^{1/2} + 1/\left(n_{2_e}\right)^{1/2}\right]} \tag{7}$$

where $\overline{x_1}$ and $\overline{x_2}$ are the averages of the variables being compared, $n_{1_e}$and n_{2_e} are the equivalent samples sizes considering auto correlation and s is the pooled sample variance. This variance, for samples sizes n_1 and n_2 for $x_1$and x_2 respectively, is given by:

$$s^2 = \frac{\left[\sum_i^{n_1}\left(x_{1_i} - \overline{x_1}\right)^2 + \sum_i^{n_2}\left(x_{2_i} - \overline{x_2}\right)^2\right]}{(n_1 + n_2 - 2)} \tag{8}$$

where the samples sizes n_1 and n_2 are considered as the sum of the number of polluted and pristine DSD parameters being compared (e. g. number of polluted and pristine stratiform D_m). To obtain n_{1_e} and n_{2_e}, the following relation was used:

$$n_{p_e} = \frac{n_p}{\left[1 + 2\sum_{\tau=1}^{n_p - 1}\left(1 - \frac{\tau}{n_p}\right)\rho(\tau)\right]} \tag{9}$$

where $p = 1{,}2$ and $\rho(\tau)$ is the auto correlation of the parameter with time-lag of τ minutes. As the measurements frequency is 1/minute, τ is always a positive integer. The $\rho(\tau)$ is calculated simply by obtaining the correlation of the parameter with itself using a time-lag of τ.

The **t** values were checked against a pre-determined table and if the value obtained was higher than the value tabulated, then the two averages were said to be significantly different. To find the appropriate threshold for each case, the effective sample size needed to be calculated:

$$N = \frac{\left(S_1^2/n_1 + S_2^2/n_2\right)^2}{\frac{\left(S_1^2/n_1\right)^2}{n_1 - 1} + \frac{\left(S_2^2/n_2\right)^2}{n_2 - 1}}. \quad (10)$$

Where S_1 and $S_2$are the standard deviation of the two samples. The **N** parameter was then utilized to search for the appropriate tabulated threshold **t**. The levels of confidence checked were 95% and 90%. Tenório et al. (2012) used a similar approach to distinguish maritime and continental rainfall rates in JWD measurements. In this work, **N** values were, for example, approximately 45 for Stratiform Rain and 160 for Local Convection events. The Stratiform Rain **N** were notably smaller mainly due to the filtering process described in section 3.

5. Results and discussion

5.1 DSD parameterization and cluster analysis

The DSD parameterization methodology described in the previous section is efficient at representing all the filtered disdrometer data because the parameterized and measured RI were linearly correlated with R^2 = 0.9996 and have nearly no bias (Figure 2a). Note that the entire range of RI values was well represented by the parameterization with only minor underestimations between 40 mm/h and 80 mm/h measured rain rates. Islam et al. (2012) parameterized DSD data in a similar manner as conducted here and found comparable results regarding the estimation of rain rates. Figure 2b shows an example of an individual gamma fit to a measured DSD associated with a rainfall intensity of 61.75 mm/h. It's possible to note that even if the gamma parameterization doesn't capture the exact same shape of the measured one (Figure 2b), it still captures efficiently the integral parameters as shown for rain rates on Figure 2a.

The 3-dimension representation of the gamma parameterization and the results of the cluster analysis for all the data set are shown in Figure 3. Each identified group was defined based on Euclidean distances and represented by a centroid, which is given by the cluster geometric center in the defined space (not shown). It is evident that the k-means method classified each cluster primarily due to differences in the Λ parameter,

which is associated with the DSD curvature and width. This could be associated with the observation that the more intense the rainfall is, the broader the DSD will be as a result of enhanced collection processes. Only cluster number 6 was identified based on unique characteristics of *m*. Most of the data suggest a tendency to vary over a plane with greater variability in Λ and N_0 than in *m*, i.e., the DSD width and intercept had greater variability than the shape. This observation can be useful for cloud/precipitation DSD parameterization and its implementation in cloud resolving models because they provide insight into DSD variability throughout different types of precipitating systems, represented here as parameter clusters.

The clusters centroid parameters are shown in Table 1. Although all DSDs associated with RI < 1 mm/h were eliminated in the filtering process, cluster 1 had an average rain rate of 0.4 mm/h. This was allowed because the cluster analysis was applied to the parameterization of N0, *m* and Λ, which were not linearly correlated with RI. Rain rates are very sensitive to variations in these parameters. Generally, the gamma parameter values decreased with increasing precipitation rates, except for cluster 6. The most frequent clusters were also the ones associated with higher RI and responsible for nearly 80% of the total accumulated rain. The centroid DSDs are shown in Figure 4, normalized by TDC in 4a and as concentrations ($mm^{-1}m^{-3}$) in 4b.

# Cluster	N_0 ($mm^{-1-m}m^{-3}$)	m	Λ (mm^{-1})	RI (mm h^{-1})	Rain Accum. (mm)	Frequency (%)
1	1.3E+15	25.6	30.2	0.4	1.6 (0.6%)	2.8
2	9.6E+09	16.4	17.5	1.4	4.6 (1.8%)	5.9
3	2.7E+07	10.6	11.7	1.8	11.2 (4.2%)	13.5
4	6.0E+05	7.8	8.2	2.3	29.1 (11.1%)	21.3
5	3.8E+04	5.2	5.5	3.7	82.4 (31.5%)	30.2
6	4.8E+01	14.6	6.2	2.8	5.9 (2.2%)	2.8
7	2.5E+03	3.2	3.3	6.3	126.9 (48.5%)	23.5

Table 1: centroid parameters of the clusters shown in Figure 4.

Figure 4a shows that a large difference between the centroid DSDs was related to the concentration of small droplets with diameters approximately 1 mm. With the exception of cluster 6, as the rainfall rate increased, their concentration decreased. For clusters 5 and 7, associated with the highest RI, there was a secondary peak in the normalized DSDs, demonstrating that these cases consisted of a combination of two droplet populations with diameters approximately 1 mm and 2 mm. Those two clusters also

present the highest relative concentrations of droplets with diameters around 0.5 mm, which can be due to a combination of droplet breakup during collisions and increased acoustic noise on the disdrometer because of the greater rainfall intensity and droplet sizes. Cluster 6 had the smallest value of N_0 and was associated with the lowest TDC (Figure 4b). This group is also representative of the greatest droplets observed (Figure 4a). However, cluster 6 had little contribution to the total accumulated rain. Moreover, the smallest droplets observed are mainly represented by cluster 1, which also had a low frequency of occurrence and the smallest relative contribution to the total rainfall. With the exception of clusters 1 and 6 (the least frequent), Figure 4b shows a general tendency of lower TDC and broader DSDs following increases in RI. This is a result of DSD reorganization inside clouds with different environmental conditions. For example, clouds forming in a stable atmosphere tend to produce light rain with DSDs closer to that of centroids 1, 2 or 3. As instability increases, collection effects (e.g., collision-coalescence, accretion and aggregation) become more efficient, favoring fast droplet growth and also droplet breakup so the result is a broader DSD. The bimodal shape of a normalized DSD is an indication that two droplet populations coexist, one with mean diameters around 1 mm and the other with the greater droplets formed by enhanced collection processes. Note that clusters 1 through 3 had similar normalized DSDs with only one peak (4a) near 1 mm in diameter. Cluster 4 had a transition between clusters 1 and 3 and the bi-modal characteristics seen in clusters 5 and 7. Although cluster 6 had a broad DSD, it was not associated with high precipitation rates because of its low TDC. This cluster was likely associated with the beginning of convective precipitation events, in which large droplets and low concentrations are often observed.

For each daily pattern classification, the mean cluster frequency distribution was calculated, as shown in Figure 5. The error bars represent one standard deviation. There was considerable variability due primarily to the small data set analyzed. Regardless, there were significant variations that exceed one standard deviation between daily patterns in clusters 1, 2, 6 and 7. Stratiform Rain days had the highest frequency of clusters 1 and 2, even when considering the variability in the other classified days. The same was found with Local Convection days for cluster 7. Cluster 6 was not observed on any stratiform rain day because it was associated with larger droplets that are generally only observed in convective systems.

When the least frequent clusters, i.e., 1 and 6, are not considered, Stratiform Rain days had a cluster frequency distribution that suggests lower values for increasing rainfall intensities. Moreover, local convection days had a frequency distribution that increased with RI. Meanwhile, organized convection days had the highest contribution in clusters

3, 4 and 5. This is an indication that both the clustering and daily classification methodologies were able to capture the essence of the precipitating system characteristics in a cohesive manner. Organized convection, as defined in the classification methodology, had both convective and stratiform characteristics, justifying the major contribution of the intermediate RI clusters. Henceforth, clusters 1, 2 and 3 will be referenced as a group of stratiform clusters. Moreover, clusters 5, 6 and 7 can be seen as convective clusters due to the association with high RI values and larger rain droplets. Cluster 4 represents a transition between stratiform and convective regimes. Note that organized convection days had the highest frequency of occurrence of this cluster, which also represents a transition from a uni- to bimodal DSD (Figure 4a).

5.2 Aerosols effects on DSD characteristics

Aerosols impacts on DSDs were analyzed through differences in D_m, TDC, RI and cluster frequency distributions between polluted and pristine precipitating scenarios for the selected events, as described in section 3. In that comparison it's assumed that the ground-based measurements of $CCN_{1.0}$ are relatively representative of the number of particles available for the activation of cloud droplets. The analysis comparing similar systems subject to different $CCN_{1.0}$ concentrations takes into account only relative variations on pollution, so the quantitative numbers of particles are not a main focus. In convective systems, the $CCN_{1.0}$ concentrations measured on ground can be representative of the number of particles inside the cloud as those systems tend to move in a direction close to the mean wind direction between 0 and 8 km of altitude (Ramsay and Doswell, 2004). As the wind also carries aerosol particles, it's fair to assume that the particles measured on the instrumentation site are representative of what is available to the system. On the other hand, stratiform systems tend to be associated with larger meteorological systems (cold fronts are fairly frequent on the Vale do Paraíba region), with distinct air masses characteristics. As such, the measurements of $CCN_{1.0}$ concentrations on the ground level should be representative, at least relatively, of the aerosol particle concentration inside those systems.

Figure 6 shows the cluster frequency distributions for polluted and pristine conditions and the respective averaged DSD for Stratiform Rain events. Note that although stratiform systems were present in clusters 5 and 7, the majority of those precipitating events were represented by clusters classified as stratiform (1, 2 and 3), in both

pristine and polluted environments. Cluster 6 was not observed in those cases because this cluster was only observed in convective rain events.

Stratiform precipitating events that were subject to higher loadings of $CCN_{1.0}$ had a higher frequency of the combined stratiform clusters (77%) and a minor participation in cluster 4. However, the pristine cases had relatively high participation in the transition and convective clusters (combination of clusters 4, 5 and 7). This suggests that aerosols favor DSDs with typical stratiform characteristics (clusters 1 to 3), preventing the formation of large droplets and heavy rainfall. In the t-Student tests, only TDC parameter presented results statistically significant when taking auto correlation into account, with a 90% confidence level. TDC was 29% higher on the polluted cases compared to the pristine ones (evidenced in Figure 6c). If auto correlation were to be disregarded, both D_m and TDC could be considered significantly different in polluted and pristine stratiform systems, with a confidence level of up to 95%. . Nevertheless, the modification in rain intensity was not statistically significant, considering or not considering auto correlation. These results suggest that TDC is the most sensible rain DSD parameter to variations in aerosol loading, which is consistent with the microphysical process of water vapor competition inside the cloud. Higher $CCN_{1.0}$ concentrations tend to allow the formation of more numerous however smaller cloud droplets, given that the liquid water path is relatively constant. Although the results presented here didn't show a statistically significant alteration of D_m in the rain DSD, it's well documented in the literature that the effects are significant on the average size of cloud droplets, which impacts rain characteristics. The results shown here are in agreement with those reported previously (e.g., Ramanathan et al., 2001; Andreae et al., 2004; Storer and van den Heever, 2013). Notably, however, the neglected large number of non-linear effects prohibits a definitive conclusion that this result is only due to the aerosol loading. It should be considered as an indication of the aerosol effect in stratiform cloud processes.

The aerosol effects on Local Convection can be seen in Figure 7. The increase in $CCN_{1.0}$ concentrations favored the convective clusters (76% of polluted cases against 53% of pristine ones), which indicates stronger rain with larger droplets. The pristine cases had a relatively high participation in the transition cluster; the polluted cases were absent in cluster 1. Figures 7c-d shows the aerosol effects on convective DSDs, which apparently favored higher D_m and lower TDC. However, the effects were only statistically significant for D_m when considering auto correlation, with a confidence level of 95%. If auto correlation is not considered, both differences of D_m and TDC would be considered significant. For RI, the difference observed between polluted and pristine

events wasn't statistically significant. The polluted D_m was 10% higher than the pristine one. This effect may be explained by an intensification of collection processes because more numerous CCN favor larger concentrations of small cloud droplets that can be collected. Therefore the precipitating droplets are larger if a sufficiently strong updraft is contained within the cloud. This result may seem contradictory to what has been reported in the literature (enhanced aerosol loading leads to smaller droplets). However, it is important to highlight that the values presented here refer to precipitating droplets and not to cloud droplets. Another important factor is that no direct classification based on vertical velocities was made for the Local Convection events. Therefore, the results shown in Figure 7 could be only partially explained by the aerosol loading. The polluted cases reported here occurred outside of the radiosonde-intensive operation in the CHUVA experiment. As a result, not enough data were available to further this analysis. These are indications of the aerosol effects on convective cloud processes. However, other non-linear effects could also contribute to the aerosol loading effects on the precipitation characteristics.

For Organized Convection cases no significant results were obtained because these systems had both stratiform and convective rain characteristics and the isolation of aerosol effects on them would be further hampered.

6. Conclusions

This work aimed to analyze precipitating events through direct measurements of their rain DSDs and CCN concentrations. The event-based DSDs were parameterized with gamma functions and presented in the 3-dimensional space domain composed by the three gamma function variables. The DSD clusters in the 3D gamma parameter domain were analyzed through a clustering method that allowed for a qualitative view of the different types of measured rain DSDs. It was found that the DSD dataset could be represented with 7 different DSD types, three could be associated with stratiform rain, three associated to convective events and one representing the transition between stratiform and convective events. This type of clustering analysis and DSD representation in the 3D gamma space can be useful for bulk microphysical models because they can be used to evaluate and adjust DSD parameterizations.

A daily rainy pattern study was carried out to identify similar environments for the formation of the precipitating systems, which were classified either as stratiform rain,

local convection or organized convection events. A good agreement was found between the clustering analysis and the daily pattern classification because the small cloud droplet clusters were predominant in stratiform rain days and large cloud droplet clusters with bimodal distributions were associated with local convection cases. Organized convection events contained both stratiform and convective characteristics and the highest mean frequency of occurrence of the transition cluster. A specific DSD, likely related to the beginning of convective events, was detected with the largest cloud droplets and the smallest total concentration.

Through the daily pattern classification, events subject to similar environmental conditions were selected, however with distinct $CCN_{1.0}$ concentrations. In this way, dynamic effects were reduced on the analysis, enabling a clearer view of the impacts of aerosols on the DSDs of the different rainfall events. An increase of approximately 200% in the concentration of $CCN_{1.0}$ was found to be associated with an increase of 29% in TDC for stratiform rain events, consistent with the mechanism of greater competition for water vapor inside the cloud as the number of aerosol particles increases. In local convective systems, an increase in aerosol loading was followed by larger rain droplets, indicating intensification of collection processes. However, additional information, including variations in convective intensities and associated vertical velocities are needed to verify if this behavior is caused by CCN effects. Nevertheless, these observations support the idea that aerosol effects on clouds and precipitation depend greatly on the precipitating system type and meteorological conditions (e.g., Khain, 2009).

The results shown were based on a field campaign. Therefore, it is a restricted dataset of rainfall events, although some interesting results presented here can serve as an indication of aerosol-cloud-precipitation effects. The changes in the DSD patterns associated with different $CCN_{1.0}$ concentrations were significant. However, the differences in precipitation rates were not significant. Although the impacts of CCN concentrations were not significant on RI, their modifications of D_m and TDC could have significant effects on cloud radiative properties, which ultimately affect climate. The clustering method in a 3D gamma parameter space is a different way to examine rain DSDs. This study should be applied to larger datasets to achieve a more statistically meaningful global characterization of different types of DSDs. Furthermore, the aerosol effects on DSD type may prove useful to formulate a conceptual model of aerosol impacts on clouds and precipitation. Expanding the results of aerosols on D_m and TDC through satellite data and/or modeling could be useful for better

understanding aerosol-cloud-precipitation feedback mechanisms and for better quantification of indirect aerosol effects on climate.

7. Acknowledgments

The author would like to thank the CHUVA experiment (project grant FAPESP 2009/15235-8) team, which enabled the development of this work, the reviewers of this paper for the insightful comments and CNPq for the financial funding.

8. References

Ackerman, A. S., Kirkpatrick, M. P., Stevens, D. E., Toown, O. B., 2004. The impact of humidity above stratiform clouds on indirect aerosol climate forcing. Nature, 432, 1014–1017, doi: 10.1038/nature03174.

Albrecht, B. A., 1989: Aerosols, Cloud Microphysics, and Fractional Cloudiness. Science, 245, 1227–1230.

Andreae, M. O., Rosenfeld, D., Artaxo, P., Costa, A. A., Frank, G. P., Longo, K. M., Silva-Dias, M. A. F., 2004. Smoking Rain Clouds over the Amazon. Science, 303 (5662): 1337-1342. doi: 10.1126/science.1092779.

Bailey, M.P., Hallett, J., 2009: A Comprehensive Habit Diagram for Atmospheric Ice Crystals: Confirmation from the Laboratory, AIRS II, and Other Field Studies. J. Atmos. Sci., 66, 2888–2899.

Freud, E., Rosenfeld, D., Andreae, M., Costa, A., Artaxo, P., 2008: Robust relations between CCN and the vertical evolution of cloud drop size distribution in deep convective clouds. Atmospheric Chemistry and Physics, 8, 1661-1675, doi:10.5194/acp-8-1661-2008.

Grandey, B. S., Stier, P., Wagner, T. M., 2013. Investigating relationships between aerosol optical depth and cloud fraction using satellite, aerosol reanalysis and general circulation model data. Atmos. Chem. Phys., 13, 3177-3184, doi:10.5194/acp-13-3177-2013.

Gunn, R., Kinzer, G. D., 1949. The terminal velocity of fall for water droplets in stagnant air. J. Meteor., 6, 243–248.

Heymsfield, A. J., McFarquhar, G. M., 2001. Microphysics of INDOEX clean and polluted trade cumulus clouds. J. Geophys. Res., 106, 28653–28673.

Igel, A. L., van den Heever, S. C., Naud, C. M., Saleeby, S. M., Posselt, D. J., 2013. Sensitivity of warm frontal processes to cloud-nucleating aerosol concentrations, J. Atmos. Sci., in press.

Islam, T., Rico-Ramirez, M. A., Thurai, M., Han, D., 2012. Characteristics of raindrop spectra as normalized gamma distribution from a Joss-Waldvogel disdrometer. Atmospheric Research 108:57-73.

Khain, A. P., 2009. Notes on state-of-the-art investigations of aerosol effects on precipitation: A critical review. Environ. Res. Lett 4, 015004.

Köhler, K., 1936: The nucleus in and the growth of hygroscopic droplets. Trans. Faraday Soc., v. 32, p. 1152 - 1161.

Lee, S. S., Donner, L., Phillips, V., Ming, Y., 2008. The dependence of aerosol effects on clouds and precipitation on cloud-system organization, shear and stability. J. Geophys. Res., 113, D16202, doi:10.1029/2007JD009224.

Lee, S. S., J. E. Penner, Saleeby, S. M., 2009. Aerosol effects on liquid-water path of thin stratocumulus clouds. J. Geophys. Res., 114, D07204, doi: 10.1029/2008JD010513.

Leinonen, J., Moisseev, D., Leskinen, M., Petersen, W. A., 2012. A Climatology of Disdrometer Measurements of Rainfall in Finland over Five Years with Implications for Global Radar Observations. Journal of Applied Meteorology and Climatology 51:392-404.

Loeb, N. G., Schuster, G. L., 2008. An observational study of the relationship between cloud, aerosol and meteorology in broken low-level cloud conditions. J. Geophys. Res., 113, D14214, doi:10.1029/2007JD009763.

Lohmann, U., Feichter, J., 2005. Global indirect aerosol effects: a review. Atmos. Chem. Phys., 5, 715-737. doi: 10.5194/acp-5-715-2005.

Machado, L. A. T., Silva Dias, M. A. F., Morales, C., Fisch, G., Vila, D., Albrecht, R., Goodman, S. J., Calheiros, A., Biscaro, T., Kummerow, C., Cohen, J., Fitzjarrald, D.,

Nascimento, E., Sakamoto, M., Cunningham, C., Chaboureau, J-P., Petersen, W. A., Adams, D., Baldini, L., Angelis, C. F., Sapucci, L. F., Salio, P., Barbosa, H. M. J., Landulfo, E., Souza, R. F., Blakeslee, R. J., Bailey, J., Freitas, S., 2013. The CHUVA Project – how does convection vary across the tropics? Submitted to Bull. Amer. Meteorol. Soc.

Marshall, J.S., Palmer, W.M., 1948. The distribution of raindrops with size. J. Meteorol. 5, 165–166.

McFiggans, G., P. Artaxo., U. Baltensperger, H. Coe., C. Facchini, G. Feingold, S. Fuzzi, M. Gysel, A. Laaksonen, U. Lohmann, T. Mentel, D. Murphy, C. O'Dowd, J. Snider. The Effect of Physical & Chemical Aerosol Properties on Warm Cloud Droplet Activation. Atmospheric Chemistry and Physics, 6, 2593–2649, doi:10.5194/acp-6-2593-2006, 2006.

Morrison, H., 2012. On the robustness of aerosol effects on an idealized supercell storm simulated with a cloud system-resolving model. Atmos. Chem. Phys., 12, 7689–7705, doi:10.5194/acp-12-7689-2012.

Petters, M.D., Kreidenweis, S.M., 2007: A single parameter representation of hygroscopic growth and cloud condensation nucleus activity, Atmos. Chem. Phys., v. 7, p. 1961–1971.

Petters, M. D., Kreidenweis, S. M., 2013. A single parameter representation of hygroscopic growth and cloud condensation nucleus activity – Part 3: Including surfactant partitioning. Atmos. Chem. Phys., 13, 1081-1091, doi:10.5194/acp-13-1081-2013.

Quaas, J., Boucher, O., Bellouin, N., Kinne, S., 2008. Satellite-based estimate of the direct and indirect aerosol climate forcing. J. Geophys. Res., 113, D05204, doi: 10.1029/2007JD008962.

Quaas, J., Ming, Y., Menon, S., Takemura, T., Wang, M., Penner, J. E., Gettelman, A., Lohmann, U., Bellouin, N., Boucher, O., Sayer, A. M., Thomas, G. E., McComiskey, A., Feingold, G., Hoose, C., Kristjánsson, J. E., Liu, X., Balkanski, Y., Donner, L. J., Ginoux, P. A., Stier, P., Grandey, B., Feichter, J., Sednev, I., Bauer, S. E., Koch, D., Grainger, R. G., Kirkevåg, A., Iversen, T., Seland, Ø., Easter, R., Ghan, S. J., Rasch, P. J., Morrison, H., Lamarque, J.-F., Iacono, M. J., Kinne, S., Schulz, M., 2009. Aerosol indirect effects – general circulation model intercomparison and evaluation with satellite data. Atmos. Chem. Phys., 9, 8697-8717, doi: 10.5194/acp-9-8697-2009.

Ramanathan, V., Crutzen, P. J., Kiehl, J. T., Rosenfeld, D., 2001. Aerosols, Climate, and the Hydrological Cycle. Science, 294 (5549): 2119-2124. doi: 10.1126/science.1064034.

Ramsay, H. A., Doswell, C. A., 2004. Exploring hodograph-based techniques to estimate the velocity of right-moving supercells. In: Preprints, 22 nd Conf. Severe Local Storms, Hyannis, EUA, Amer. Met. Soc., digital media, 2004. (available at http://ams.confex.com/ams/11aram22sls/techprogram/paper_81131.htm).

Roberts, G., Nenes, A., 2005. A continuous-flow longitudinal thermal gradient CCN chamber for atmospheric measurements. Aeros. Sci. Tech., 39, 206–221, doi: 10.1080/027868290913988.

Rosenfeld, D., Lohmann, U., Raga, G., O'Dowd, C., Kulmala, M., Fuzzi, S., Reissell, A., Andreae, M., 2008. Flood or drought: how do aerosols affect precipitation? Science, 321, 1309, doi: 10.1126/science.1160606.

Rosenfeld, D., 2000. Suppression of rain and snow by urban and industrial air pollution. Science, 287, 1793–1796, doi: 10.1126/science.287.5459.1793.

Smith, J. A., 1993: Marked point process models of raindrop-size distributions. J. Appl. Meteor., 32, 284–296.

Smith, J. A., R. D. De Veaux, 1994: A stochastic model relating rainfall intensity to raindrop processes. Water Resour. Res., 30, 651–664.

Steiner, M., Smith, J. A., 2000: Reflectivity, rain rate, and kinetic energy flux relationships based on raindrop spectra. J. Appl. Meteor., 39, 1923–1940.

Storer, R. L., van den Heever, S. C., 2013. Microphysical processes evident in aerosol forcing of tropical deep convection, J. Atmos. Sci., 67, 430–446.

Storer, R. L., van den Heever, S. C., Stephens, G. L., 2010. Modeling aerosol impacts on convective storms in different environments, J. Atmos. Sci., 67, 3904–3915.

Tenório, R. S., Cristina da Silva Moraes, M., Sauvageot, H., 2012. Raindrop Size Distribution and Radar Parameters in Coastal Tropical Rain Systems of Northeastern Brazil. Journal of Applied Meteorology and Climatology 51:1960-1970.

Tokay, A., Short, D. A., 1996. Evidence from Tropical Raindrop Spectra of the Origin of Rain from Stratiform versus Convective Clouds. J. Appl. Meteor., 35, 355–371. doi: http://dx.doi.org/10.1175/1520-0450(1996)035<0355:EFTRSO>2.0.CO;2

Tokay, A., Kruger, A., Krajewski., W. F., 2001. Comparison of drop size distribution measurements by impact and optical disdrometers. Journal of Applied Meteorology 40:2083-2097.

Twohy, C. H., Petters, M. D., Snider, J. R., Stevens, B., Tahnk, W., Wetzel, M., Russell, L., Burnet, F., 2005. Evaluation of the aerosol indirect effect in marine stratocumulus clouds: Droplet number, size, liquid water path, and radiative impact. J. Geophys. Res., 110, D08203, doi: 10.1029/2004JD005116.

Twomey, S. A., 1974. Pollution and planetary albedo. Atmos. Environ., 8, 1251–1256.

Uijlenhoet, R., Steiner, M., Smith, J.A., 2003. Variability of raindrop size distributions in a squall line and implications for radar rainfall estimation. J. Hydrometeorol. 4, 43–61.

van den Heever, S. C., Carrió, G. G., Cotton, W. R., DeMott, P. J., Prenni, A. J., 2006. Impacts of nucleating aerosol on Florida storms. Part I: Mesoscale simulations. J. Atmos. Sci., 63, 1752– 1775.

van den Heever, S. C., Stephens, G. L., Wood, N. B., 2011. Aerosol indirect effects on tropical convection characteristics under conditions of radiative-convective equilibrium. J. Atmos. Sci., 68, 699–718, doi: 10.1175/2010JAS3603.1.

Zwiers, F. W., von Storch, H., 1995. Taking serial correlation into account in tests of the mean. J. Climate, 8, 336–351.

Figures

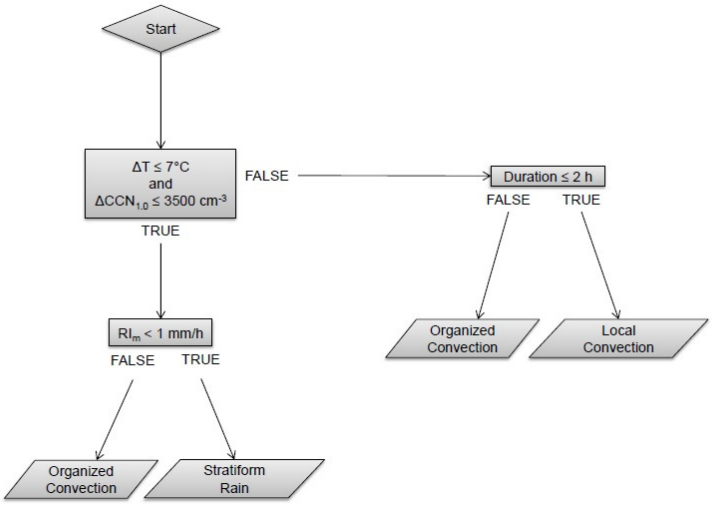

Figure 1 - Decision tree for the daily pattern classification. Rectangular blocks represent condition checks.

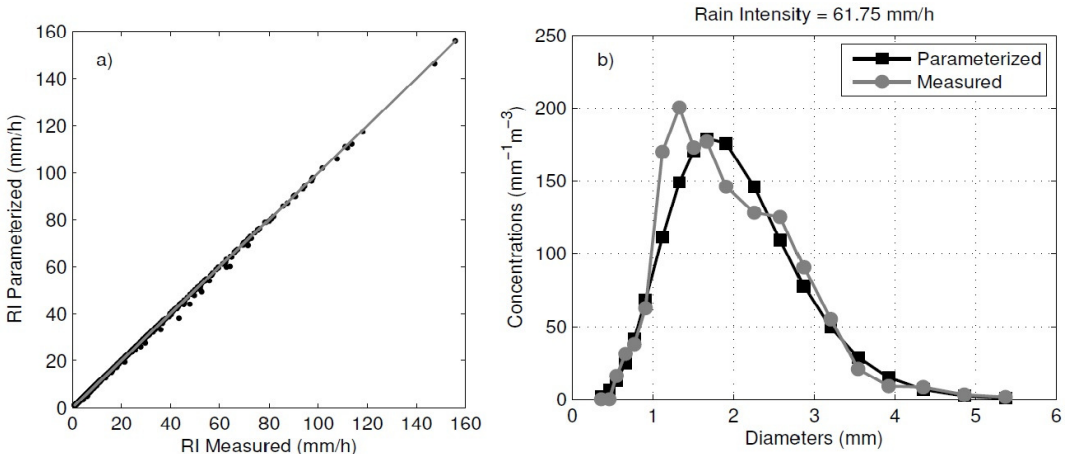

Figure 2 - Parameterized rain rate against measurements. The line represents the perfect linear fit (1 x 1).

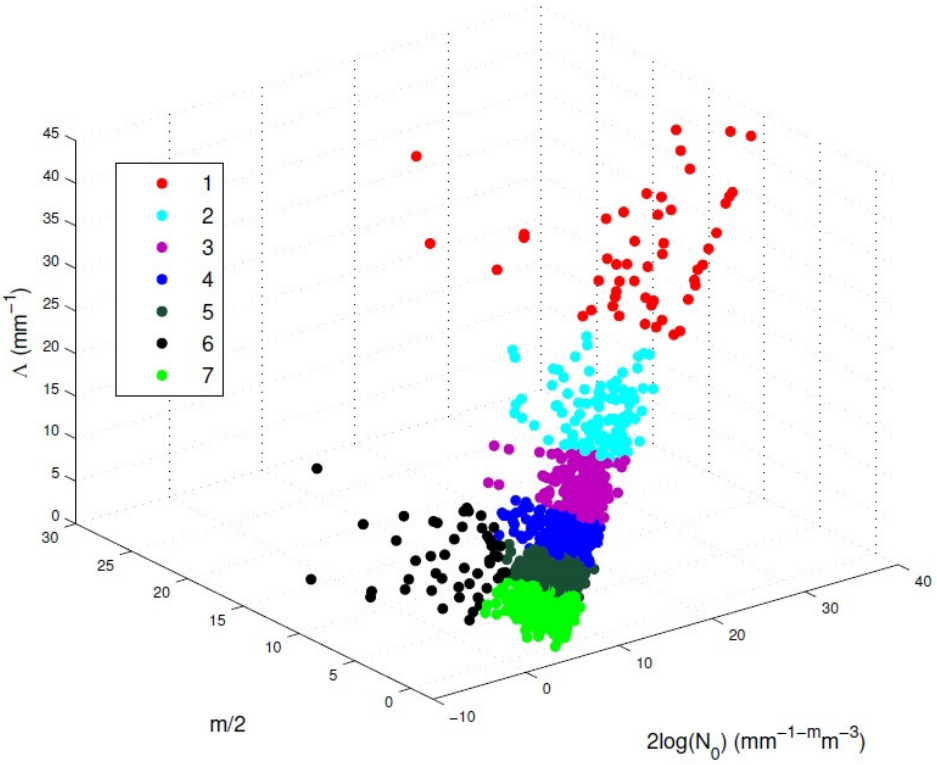

Figure 3 - The 3-dimension domain for the gamma function parameterization and visualization of the 7 clusters identified using the k-means method. The legend associates one number to each cluster.

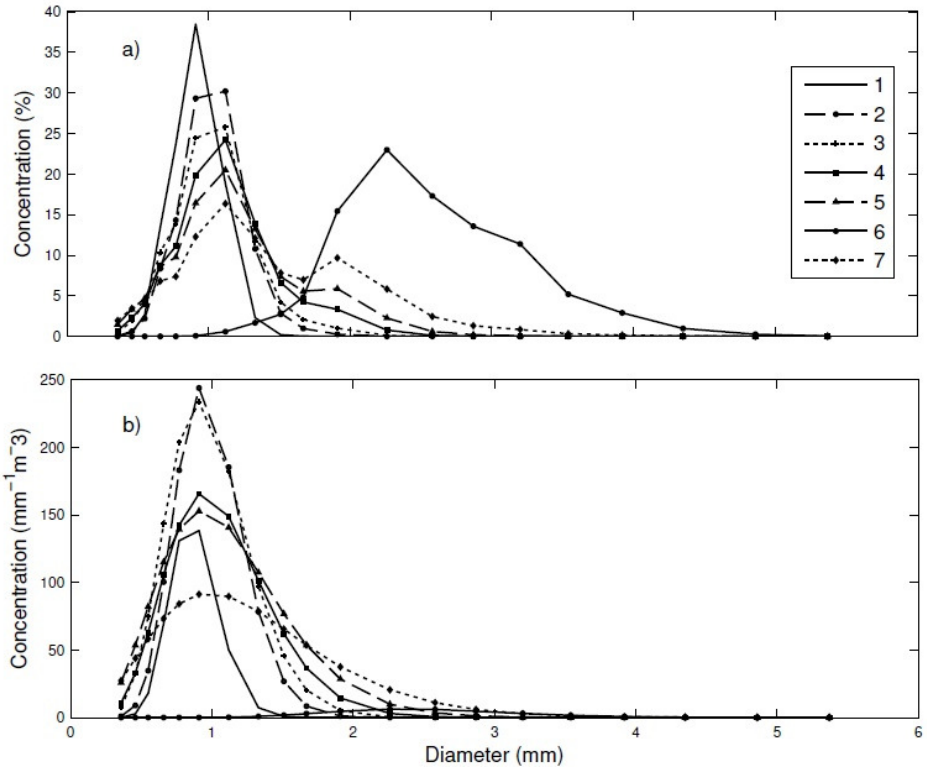

Figure 4 - Centroid DSDs a) normalized by TDC and b) as concentrations per size bin.

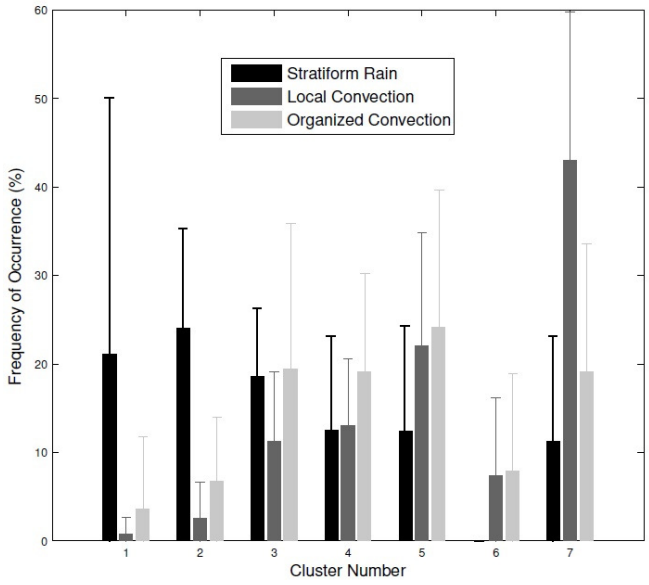

Figure 5 - Mean cluster frequency distributions for local convection, organized convection and stratiform rain days. Error bars represent one standard deviation.

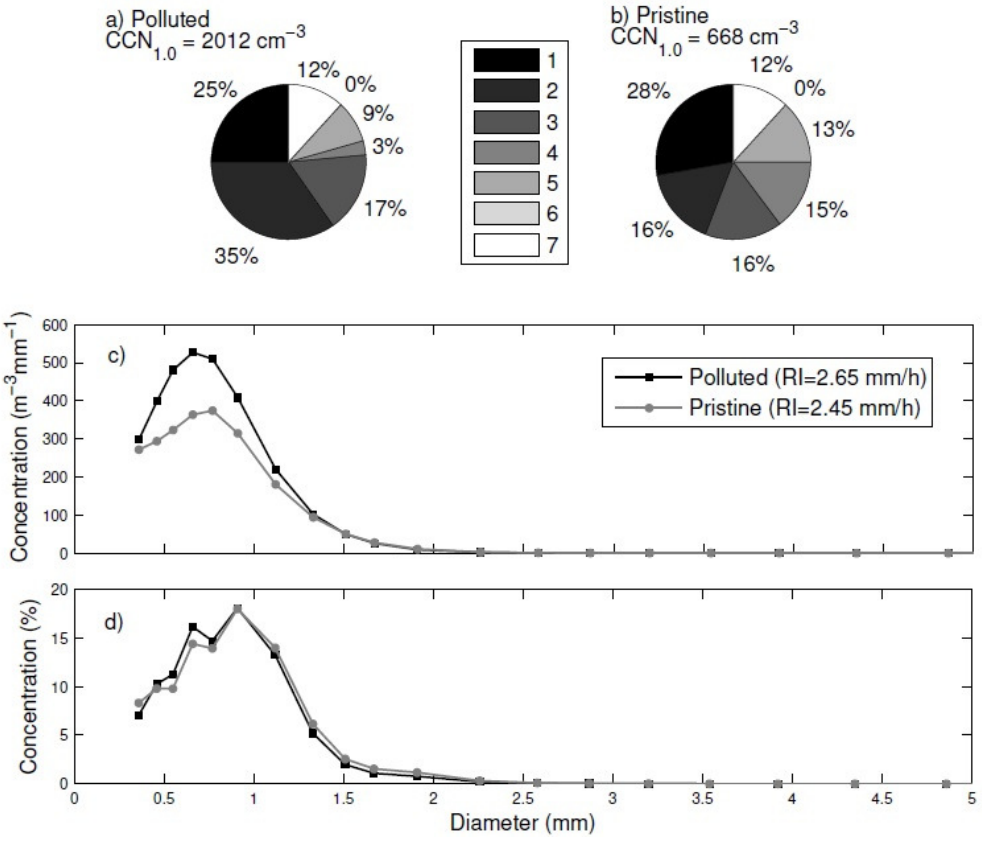

Figure 6 - Cluster frequency distributions for relatively a) polluted and b) clean stratiform events. Averaged DSDs for polluted and pristine events c) in concentration per size bin and d) normalized by TDC. The CCN concentrations reported are the averages for the two polluted and two pristine cases.

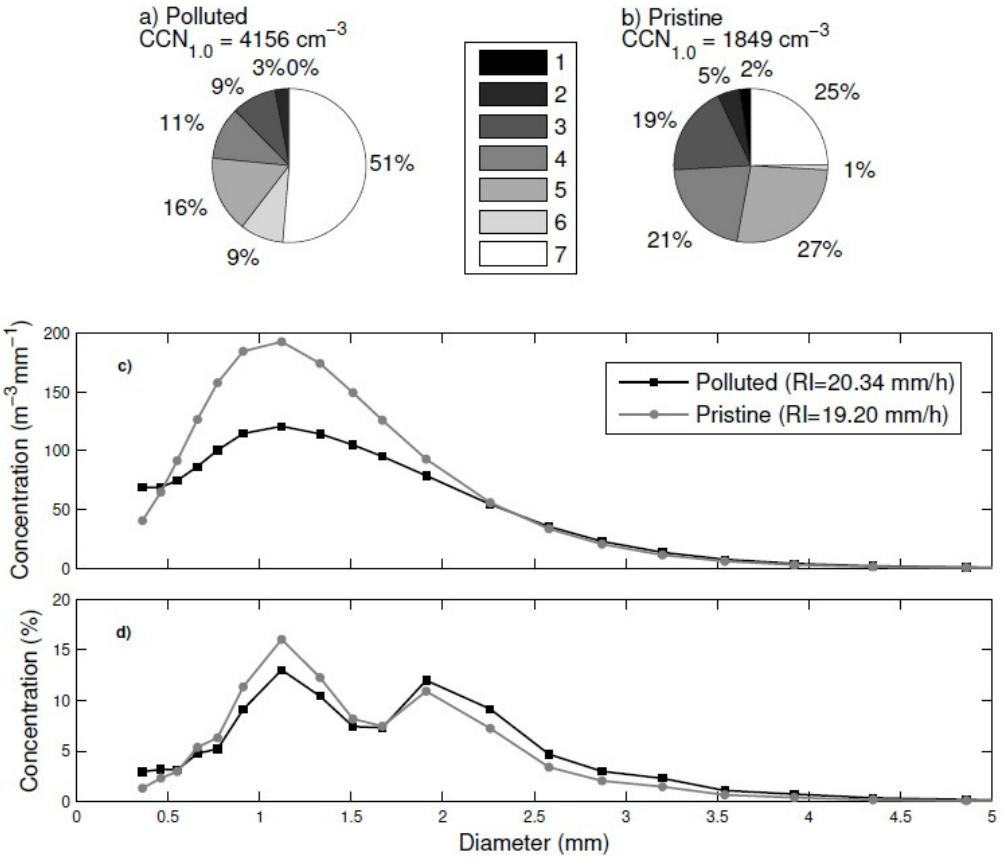

Figure 7 - Similar to Figure 6, except for the local convection cases.